Supporting Information

Self-Powered Human Interactive Transparent Nanopaper Systems

Junwen Zhong [1,§], Hongli Zhu[2,§], Qize Zhong [1,§], Jiaqi Dai[2], Wenbo Li[1], Soo-Hwan Jang[2], Yonggang Yao[2], Doug Henderson[2], Qiyi Hu[1], Liangbing Hub[2,] and Jun Zhou[1,*]*

[1]Wuhan National Laboratory for Optoelectronics, and School of Optical and Electronic Information, Huazhong University of Science and Technology, Wuhan, 430074, China.

[2]Department of Materials Science and Engineering, University of Maryland, College Park, Maryland, 20742, US

[§]J.W.Z., H.L.Z. and Q.Z.Z. contributed equally to this work.

* Correspondence authors: jun.zhou@mail.hust.edu.cn(JZ) and binghu@umd.edu(LBH)

Supporting Figures

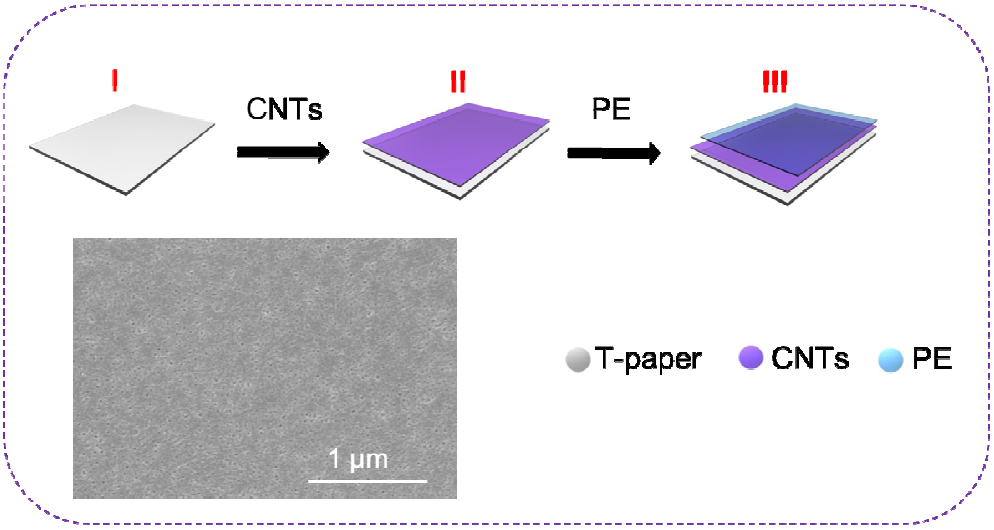


Figure S1 Fabrication process of carbon nanotubes (CNTs)/transparent nanopaper (T-paper) and polyethylene (PE)/CNTs/T-paper components. Insert Scanning Electron Microscope (SEM) image shows the surface topography of the transparent nanopaper.

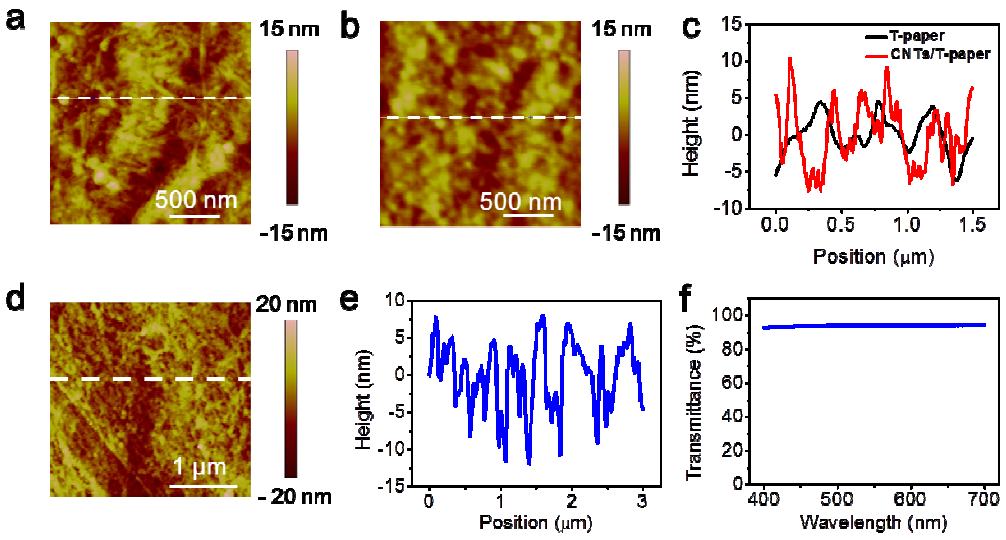


Figure S2 Atomic force microscope (AFM) images of the surface of (a) CNTs/T-paper and (b) transparent nanopaper, respectively. (c) Relative altitudes along the white lines in (a) and (b), respectively. (d) AFM image of the surface of PE film. (e) Relative altitude along the white line in (d). (f) Transmittance of PE film in visible light range.

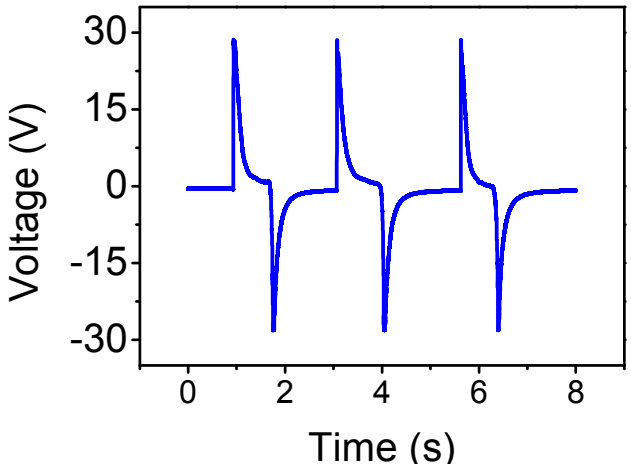


Figure S3 The open-circuit voltage for the transparent paper-based flexible generator (TPFG) stimulated by finger pressing.

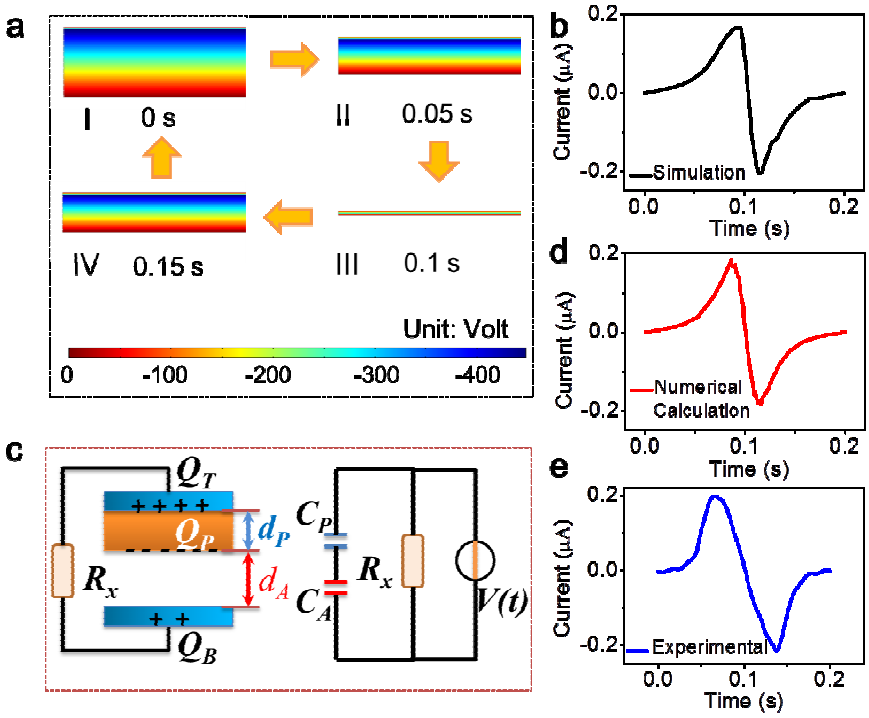


Figure S4 COMSOL simulation and theoretical analysis. (a) Finite element simulation of periodic potential change of a TPFG. (b) Current signal based on a finite element simulation. (c) Equivalent electrical circuit model of a TPFG. Current signals (d) calculated from numerical calculation and (e) measured by experiment.

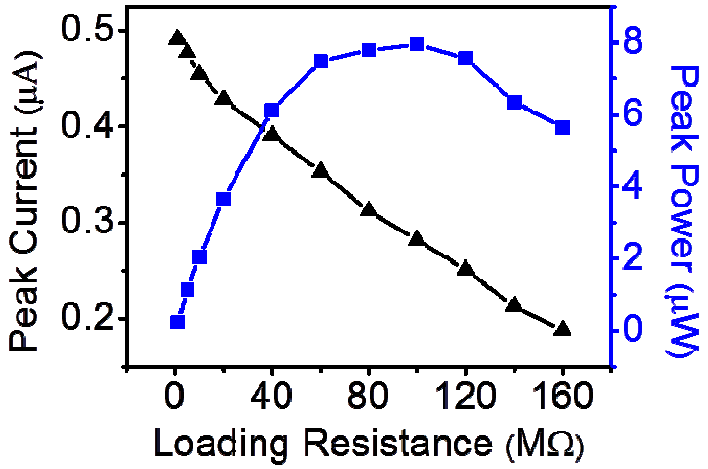


Figure S5 Loading peak currents and power of a TPFG with different external load resistances at a given stimulated frequency of 5 Hz and amplitude of 2.5 mm.

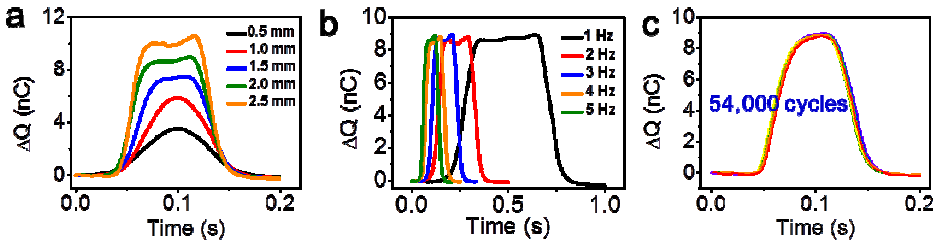


Figure S6 Transferred charges of a TPFG (a) varied with stimulated amplitude of 0.5, 1, 1.5, 2, and 2.5 mm for a given frequency of 5 Hz and (b) varied with stimulate frequencies of 1 Hz, 2 Hz, 3 Hz, 4 Hz and 5 Hz for a given amplitude of 2 mm. (c) Transferred charges over time of a TPFG continuously working for 54,000 cycles.

Supporting calculation

Working mechanism analysis based on a finite element simulation.

To explore the generation mechanism of the generator working in a cyclic vibration, a finite element simulation (COMSOL Multiphysics software) was introduced. The constructed model was based on a real size of a TPFG, and the simulated background was in free space of air. In this work, the air gap between the two components has a key role in the generation of this electric current. Therefore, to analyze this mechanism, the bottom component was assigned as a cosine mode of motion, the expression of which is as following:

$$d_A(t) = 0.5d_A[1+\cos(\omega t)] \quad (1)$$

Where d_A is the thickness of the air gap at t=0, and ω is the angular frequency of the cosine wave.

The computed results of electrical potential distribution at different moment caused by electrostatic induction are schematically depicted in **Figure S4a**. As the bottom component was in non-compressed phase (**Figure S4a_I**), $V_T = V_B$ (V_T and V_B represent the surface potential of the PE/CNTs/T-paper component electrode and CNTs/T-paper component electrode, respectively), and no free electrons would flow in the external circuit. When the vertical compression of the cosine motion was applied to the device, the equilibrium state was broken. From the observation of **Figure S4a-II**, the top electrode had a higher potential which would drive the electrons flowing from the bottom electrode to the top one when the generator was in short circuit. In this case, the current was generated. With the compression increased, more electrons were accumulated in the top electrode to balance the potential

difference, as illustrated in **Figure S4a-III**. In the relaxation process (**Figure S4a_IV**), then $V_T < V_B$, which would result in the electrons flowing back to the bottom electrode and creating an opposite signal. Therefore, the motion of bottom component is oscillating at an angular frequency ω, the two electrodes will continuously charge and discharge at different phases relative to each other, which produce an alternating current through the external circuit, which is shown in **Figure S4b**. In order to indicate the working mechanism more vividly, the dynamic simulation process is shown in **Video 3**.

Theoretical analysis and its numerical solution.

Under the comprehension of the simulation, it is possible to express the theories of the generation mechanism with an equivalent electrical circuit model illustrated in **Figure S4c**, where our TPFG is considered as two independently ideal parallel flat-capacitors, which were connected in subtractive series. In this prototype, we assume that C_P and C_A represent the capacitors of the top region with PE film dielectric and the bottom region with air dielectric, respectively. According to flat capacitance formula, we can obtain an expression for the capacitances C_P and C_A, respectively:

$$C_P = \frac{\varepsilon_{rp}\varepsilon_0 S}{d_P} \tag{2}$$

$$C_A(\mathrm{t}) = \frac{\varepsilon_0 S}{d_A(\mathrm{t})} \tag{3}$$

Here d_P is the thickness of PE film with its dielectric constant of ε_{rp}, S is the contact area. It is noting that the air gap d_A(t) could be mechanically constrained by vertically vibrating the bottom component in accordance with the form of a cosine wave, which could be described

as follow according to the real test equipment:

$$d_A(\mathrm{t}) = 0.5d_A[1+\cos(\omega \mathrm{t})]+\Delta d \tag{4}$$

Where ω is the controlled angular frequency of the cosine wave, Δd represents the correct factor of the cosine wave amplitude which is related with ω in our equipment.

According to Kirchhoff Voltage Law and Ohm's law, the output voltage of the generator is given by:

$$V(\mathrm{t}) = \frac{Q_T(\mathrm{t})}{C_p} - \frac{Q_B(\mathrm{t})}{C_A(\mathrm{t})} \tag{5}$$

$$V(\mathrm{t}) = I_x R_x = \frac{\partial Q_B(\mathrm{t})}{\partial \mathrm{t}} R_x \tag{6}$$

Where $Q_T(\mathrm{t})$ is the quantity of positive charge produced on the top electrode and $Q_B(\mathrm{t})$ is that of the bottom electrode due to electrostatic induction.

Combine Eqn. (2), (3), (5) and (6), we can get:

$$\frac{Q_T(\mathrm{t})d_p}{\varepsilon_{rp}\varepsilon_0 s} - \frac{Q_B(\mathrm{t})d_A(\mathrm{t})}{2\varepsilon_0 s} = \frac{\partial Q_B(\mathrm{t})}{\partial \mathrm{t}} R_x \tag{7}$$

In the experiment, the negative charge on the PE film is injected by corona method, whereas $Q_B(\mathrm{t})$ and $Q_T(\mathrm{t})$ are caused by electrostatic induction, so we can express the value of Q as follow:

$$-Q = Q_T(\mathrm{t}) + Q_B(\mathrm{t}) \tag{8}$$

The surface potential has been tested by electrometer for nearly a month and the graph is plotted in **Figure 3a**, which can maintain a narrow fluctuation near - 550 V after several weeks of natural attenuation.

Combine above equations, and then we can get:

$$\frac{\partial Q_B(t)}{\partial t} + Q_B(t) * \left\{ \frac{d_p}{R_x \varepsilon_{rp} \varepsilon_0 S} + \frac{d_A\left[1 + \cos(\omega t)\right] + \Delta d}{2R_x \varepsilon_0 S} \right\} + \frac{Q d_p}{R_x \varepsilon_{rp} \varepsilon_0 S} = 0 \quad (9)$$

$$\text{Initial phase: } Q_B(0) = -\frac{Q d_p}{d_p + d_A(0)\varepsilon_{rp}} \quad (10)$$

$Q_B(\mathrm{t})$ can be got through solving this differential equation, and the current can be derived using the current definition:

$$I(\mathrm{t}) = \frac{\partial Q_B(\mathrm{t})}{\partial t} \quad (11)$$

Due to its complexity, a numerical calculation was introduced to solve Eqn. (9). The results are shown in **Figure S4d**. All these calculations are based on the most ideal conditions.

To further verify the simulation and the theoretical analysis, an experiment was carried out to compare the above results. The setup was similar to the experiment in our previous report. **Figure S4e** shows the current result of the experiment, the trend of which matches the numerical calculation and simulation current output profile quite well. Therefore, the estimation of the simulation or theoretical analysis is valuable and accurate.

Supporting Videos

Supporting Video 1. Transparent Paper-Based Art Anti-Theft System

Supporting Video 2. Transparent Paper-Based Smart Mapping Anti-Fake System

Supporting Video 3. Dynamic Simulation Process for A Transparent Paper-Based Flexible Generator.